Wake control through tip-speed ratio adaptation

Andreas Knauer[1], Lutz Mütschard[1], Matt Churchfield[2], Senu Sirnivas[2]

[1]Equinor ASA, Forusbeen 50, 4035 Stavanger, Norway
[2]National Renewable Energy Laboratory, 15013 Denver West Parkway, Golden, CO 80401, USA

Correspondence to: Andreas Knauer (andkn@equinor.com)

Abstract. Offshore wind farms can generate wake losses between 10 and 20% even after layout optimization. By altering the turbine operational parameters, it is possible to reduce internal wake effects. A wake-control approach by modifying the operational tip-speed ratio is presented here using LES high-fidelity modelling with DTU 10 MW reference wind turbines. Single- and two-turbine simulations for tip-speed ratios ranging from 5 to 12 are assessed for wake losses and improved power production. Simulations were conducted with non-turbulent inflow, as subtle rotor- and wake aerodynamic effects are difficult to identify in turbulent flow.

Single-turbine simulation results show that the wake development is strongly influenced by the operational tip-speed ratio. At a tip-speed ratio of 8, a stronger wake with increased turbulence and a relatively short recovery distance is observed. Tip-speed ratios greater than 8 create a more turbulent near wake, increased mixing, and the shortest recovery distance.
The tip-speed ratio influences not only the magnitude of turbulence in the wake, but also the axial position where the wake becomes fully turbulent. With increasing tip-speed ratio, the point of a fully turbulent wake state moves upwind towards the rotor, enhancing turbulent mixing and reducing wake recovery distance. At high tip-speed ratios wake turbulence dissipates faster, and downwind turbines are not exposed to increased turbulence loads. At a tip-speed ratio of 10, the minimum wind speed at 6 rotor diameters downwind is enhanced by 50 % compared to the optimal operational tip-speed ratio of 8.
An increase in net power production is observed by operating the upstream turbine at a higher tip-speed ratios compared to the downwind turbine operating at the tip-speed ratio of 8. The net power production increases up to 10 %.

These results demonstrate the potential of varying tip-speed ratio to control wake development to maximize net power production of turbine arrays. Furthermore, turbulence-induced loads can be modified with this control strategy. These proof-of-concept simulations show the interesting potential of tuning the operational tip-speed ratio for wake control.

1 Introduction

Wind conditions offshore are often favorable for energy production due to consistently higher wind speeds compared to onshore wind parks (Badger et al., 2025). The established practice is to create offshore wind parks which contain large numbers

of turbines operating in close vicinity. The turbines are exposed to a completely different wind environment compared to an isolated, single turbine. In wind parks, complex turbine–wake interactions are typical, decreasing performance and increasing mechanical fatigue loads (Thomsen, K. and Sørensen, P., 1999) (Méchali et al., 2006). In offshore wind farms, wake effects are generally stronger compared to onshore wind farms. Onshore, terrain-induced and daytime convective turbulence often cause relatively fast wake recovery compared to offshore. Offshore wakes are more persistent because of lower effective surface roughness and often stably stratified atmospheric conditions, both of which lead to lower turbulence intensity and decreased wake mixing. Offshore wind farm layouts are optimized to minimize the impact of wake effects, but typically 10–20 % of the power production is lost due to internal wake effects (Barthelmie et al., 2009). In tightly spaced parks, the losses can be even higher; losses of up to 28 % are observed at the Lillgrund wind farm (Sebastiani et al., 2021).

Wake control has the potential to reduce wake losses, increasing power production. Furthermore, turbines subject to turbulent wakes experience increased fatigue loads, which may incur maintenance costs, so reducing wake effects can decrease these maintenance costs. Both effects influence the levelized cost of energy (LCOE). Reduced maintenance costs decrease the numerator of the LCOE equation, and increased power production increases its denominator, both of which act to reduce LCOE.

For existing wind farms, the wake development can be modified by changing the operational parameters for the turbines. Common techniques include yaw control/wake steering, axial induction modification, active wake control, rotor aerodynamics for wake modification, and combinations of these. Research activities in the last decade have increasingly focused on wake control and various countermeasures to limit the impact of wake effects. Comprehensive overviews of wake management techniques are given by (Houck, 2022) (Boersma et al., 2017) (Munters, W. and Meyers, J., 2018).

In this work, we focus on axial induction control, which modifies the induction factor of an upstream turbine, through modification of the rotor tip-speed ratio (TSR), which is the ratio of the linear speed of the blade tips to the inflow wind speed. This can be achieved by modifying the generator torque controller. The axial induction factor can also be controlled through blade pitch angle. The goal of axial induction control is to increase downwind wake velocities by modified upstream turbine operation. If the power production and the related thrust are reduced, a downstream turbine in the wake will experience higher wind speeds, resulting in increased power production.

In wind tunnel tests with small-scale models (Adaramola, 2011), the effects of power extraction and downwind distance on the production of a downwind turbine are demonstrated. The power loss of the downwind turbine varied from 20 % and 46 % when compared to the unobstructed turbine operating at design conditions. The impact of the operational TSR on the wake development and the power production of a turbine in the wake is shown. For both higher and lower TSRs, the power production of the downwind turbine is increased by 21% (high TSR), and 26% (low TSR), respectively. The results identify a

clear potential: the tuning of the operational TSR can increase downwind turbine efficiency. (Porté-Agel, F. and Dillip, D., 2017) demonstrates production gains of up to 2.8% for pitch variations in a low turbulence environment for a two-turbine array using high-fidelity, turbulence-resolving fluid flow simulations. Furthermore, the effect of turbulence intensity of the inflow is addressed.

The sensitivity of wake deflection technologies to wind direction variability and uncertainty was investigated by (Rott et al., 2018) They devise a yaw control method for active wake deflection which accounts for changing wind direction and uncertainty in wind direction measurements. Their research shows that, under realistic inflow conditions, the control algorithm can be customized to specific wind farm and atmospheric conditions, resulting in an overall power increase. (Bossanyi, E. and Ruisi, R., 2021) optimize the flow for a turbine row through the application of an optimizer in the LongSim program. New operational set points are generated and applied to one row at the Sedini wind farm. The number of extracted data points is relatively low but indicates an average power increase between 1.7 % and 2.4 %. The application of wake steering in the design phase for a complete offshore wind farm was assessed by (Fleming et al., 2022). The model FLORIS was used with a Serial-Refine algorithm for the accelerated identification of optimal yaw angles for wake deflection.

The simulated and observed concepts to mitigate wake losses vary in their efficiency but demonstrate that a wind turbine wake, despite is complexity, can be modified. In this work, we explore the modification of operational TSR to reduce wake effects and increase power production. The remainder of this article is organized as follows: Section 2 describes the 10 MW wind turbine model central to this study, Section 3 describes the engineering rotor aerodynamics and high-fidelity large-eddy simulation tools we use, Section 4 explores the effect of TSR modification on power production using the engineering rotor aerodynamics tool, Section 5 explores large-eddy simulation of a single wake under modified TSR operation, Section 6 explores two turbines – one waked by the other – under modified TSR operation, and Section 7 provides conclusions.

2 Wind turbine model

The 10 MW reference wind turbine (referred to as the DTU 10 MW turbine) developed at the Technical University of Denmark (DTU) is used in this study. A report by (Bak et al., 2012) gives a description of the aerodynamic and aeroelastic model data. The turbine is modelled in the QBlade (Marten, 2024) and OpenFAST (Jonkman, 2024) programs.

The DTU rotor represents a good starting point for parameter studies with a large, efficient turbine. The rotor is a product of a design process focusing on a lightweight, robust blade with iteration loops through aerodynamics, structural design, and aeroelastic load calculations. The rotor is suitable for these wake studies because of its performance and robustness. The overall characteristics of the DTU 10 MW turbine are summarized in Table 1.

Table 1: Overall characteristics of the DTU 10 MW turbine.

Parameter	Value
Rated power	10 MW
Cut-in power	4 ms^{-1}
Rated wind speed	11.4 ms^{-1}
Cut-out wind speed	25 ms^{-1}
Rotor diameter	178.3
Rotor speed	6 to 9 rpm, up to 10 in actual tests
Hub height	119 m
Drivetrain	Medium-speed, multi-stage gearbox
Hub overhang	7.1 m
Shaft tilt angle	5.0 deg.
Rotor mass	227,962 kg
Nacelle mass	446,036 kg

3 Numerical models

3.1 Rotor aerodynamic analysis: QBlade

We use the QBlade rotor design module for our rotor aerodynamics performance parameter studies. This tool allows a fast, high-quality check and tuning of the aerodynamic rotor parameters. QBlade is a multi-physics wind turbine simulation code used for aeroelastic analysis and certification. The development of QBlade began in 2010, and it is maintained by the Technical University of Berlin. The code is written in modern, modular, object-oriented C++, and it encompasses efficient multi-fidelity aerodynamics, structural dynamics, and hydrodynamics.

QBlade is performance portable, running on modern CPU and GPU hardware through OpenMP and OpenCL parallelization. The thoroughly validated aerodynamic modules include lifting-line, free-vortex wake methods. The rotor wake is modelled using Lagrangian vortex elements instead of steady-state blade-element momentum (BEM) theory, providing more accurate and detailed spatio-temporal predictions of the rotor induction and wake velocity field. The aerodynamics of horizontal-axis wind turbines can also be simulated using an unsteady polar-BEM implementation. With this tool, we can study wind turbine wake effects, even for the more complex case of offshore floating turbines with floater motion. However, the turbulence development cannot be assessed with these vortex methods because of their limitations in resolving the turbulent spectrum and its spatial and spectral development.

3.2 High-fidelity fluid flow simulation: SOWFA

For high-fidelity flow simulations of wind turbine wakes, we employ computational fluid dynamics (CFD). More specifically, we perform large-eddy simulation (LES), in which we directly resolve the larger, energy-containing turbulent scales, and model the effects of the unresolved smaller scales. LES is linked to Kolmogorov's 1941 theory of self-similarity, which suggests that larger eddies are shaped by flow geometry and anisotropic, whereas the smaller eddies are more universal and isotropic; therefore, it is best to directly resolve the larger eddies and model the smaller ones. To perform LES, we use the Simulator fOr Wind Farm Applications (SOWFA) (Churchfield, 2024) developed and maintained by the National Renewable Energy Laboratory (NREL). SOWFA is a collection of wind-energy-specific libraries and a solver built on the OpenFOAM CFD toolbox (OpenCFD, 2025). SOWFA solves the incompressible, non-hydrostatic form of the fluid flow equations that include the Boussinesq approximation for buoyancy effects, one of the most used formulations for atmospheric LES. The code discretizes the governing equations on a fully unstructured mesh using an implicit temporally and spatially second-order accurate finite-volume method. The equations are solved sequentially but are coupled through an outer iteration loop. The turbulence model used is that of (Moeng, 1984). As is common in wall-bounded high-Reynolds-number LES, the turbulence is not fully resolved in the first grid layer adjacent to the surface; hence, we perform wall-modelled LES and employ Schumann and Grötzbach's (Schumann, 1975) (Grötzbach, 1987) surface shear stress and heat flux model where the connection between fluxes and the velocity and temperature profiles comes from Monin–Obukhov similarity theory. The rotor aerodynamics are modelled using an actuator line representation of the rotor that is coupled to the NREL OpenFAST aero-servo-elastic code (Jonkman, 2024). SOWFA allows the investigation of wind turbine performance and wake development under the full range of atmospheric conditions and in complex terrain.

LES of wind turbine wakes in an offshore farm is computationally expensive and requires high-performance parallel computing. SOWFA simulations are performed on NREL's Kestrel cluster, an Azure Cloud cluster, and an Equinor in-house cluster. Typical cases with computational domains of 2200 m x 800 m x 800 m and five refined grid levels have up to 43 million cells and require approximately 50,000 CPU-hours for the typical 600 s simulation.

4 Variation of the tip-speed-ratio

Wind turbine rotor blades are tuned for optimal energy extraction. A TSR is chosen to maximize coefficient of power but is often constrained by a maximum tip speed to avoid excessive noise generation. Twist and chord length are typically tuned such that the airfoils along much of the blade length operate at maximum lift-to-drag ratio for the design TSR. A modification of the operational TSR can adversely affect the efficiency of a designed and optimized rotor. The power coefficient of the DTU 10 MW turbine as a function of the operational TSR is shown in Figure 1.

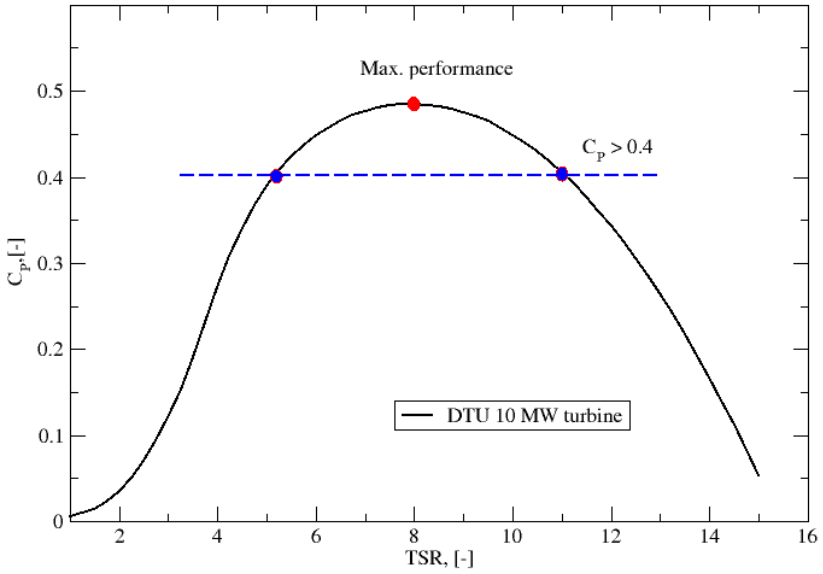

Figure 1: Power coefficient vs TSR for the DTU 10 MW turbine from a Qblade simulation.

The operation at different off-design TSRs and the impact on aerodynamic parameters is shown in Figure 2. The main aerodynamic effects are:

- Low-TSR operation establishes higher angles of attack, but because of the quadratic impact of the velocity, reduced lift and a lower axial induction. The flow over a section is likely more unstable compared to the original operational point.
- High-TSR operation creates decreased angles of attack, but enhances the high lift force development and high axial induction due to increased velocities. The flow on the rotor is more stable; lower angles of attack will decrease the occurrence of stall.

With respect to aerodynamic stability, high-TSR operation is preferred because the outer sections extract more momentum from the flow and create a stronger radial gradient of streamwise velocity across the wake and at the wake edges. This velocity gradient is a key quantity in the production term of turbulent kinetic energy; therefore, one may expect stronger wake turbulence development and hence mixing of high-momentum freestream flow back into the wake. Along these lines, the operation at slightly increased TSRs to control the wake development is evaluated in this work.

A comparison is made for operations at three TSRs (6, 8, and 10). The aerodynamics of the rotor rely on the aerodynamic performance of the rotor sections. Figure 2 shows radial distributions of angle of attack (left) and lift-to-drag ratio (right). If the rotor is operated at TSR 6, the angle of attack increases considerably for all sections. For radial positions up to 30 m, angles of attack larger than 15 degrees appear, and stall effects can be expected. The lift-to-drag ratio is quite low here – airfoils near stall do not work optimally. For the outer sections, the aerodynamic performance is better. However, the sections operate at angles of attack between 10 and 15 degrees, which is near maximum lift and possible stall. Overall, rotor performance and stability of the flow are reduced at lower TSRs.

As expected, the results for the operation at TSR 8 show the best performance. The DTU rotor design appears to be aerodynamically optimized for a TSR of 7.5, but the operation of the rotor slightly above the design TSR ensures a broader band of good efficiency. Here, the airfoils are operated at angles of attack between 5 and 10 degrees, where their best performance (lift-to-drag ratio) occurs.

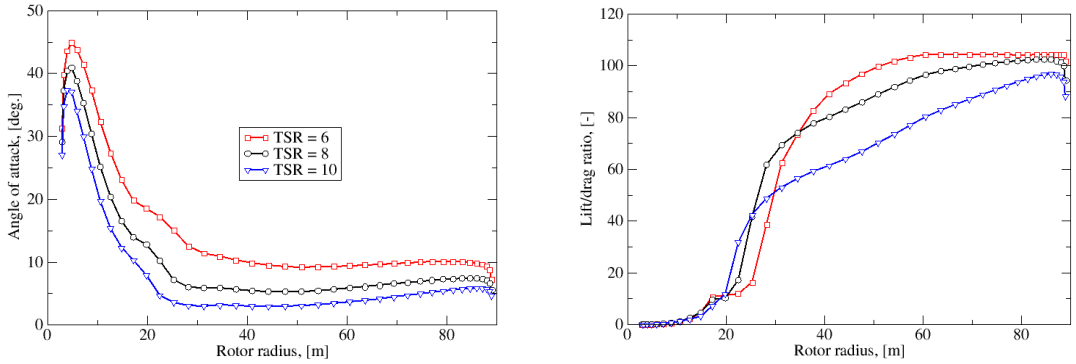

Figure 2: Angle of attack vs rotor radius (left) and lift-to-drag ratio vs rotor radius (right) for different TSRs.

For the operation at TSR 10, angles of attack are reduced for all blade sections. This increases flow stability and resistance against stall effects. However, the airfoils/blade sections do not work at their maximum lift-to-drag ratio, see Figure 2. The effect is caused by a lift reduction, and drag is approximately at the same level. It is obvious that the operation at TSR > 8 reduces the rotor performance slightly, but that comes with the positive benefit of increased flow stability on the blades. This could be beneficial, for example, in a high-velocity shear or turbulence environment where angle-of-attack variation over time is increased, because operating at a lower angle of attack increases the margin before stall. Another effect of high-TSR operation is the increased Reynolds number, which increases the overall airfoil and rotor performance. However, Reynolds number effects are not assessed here.

For higher operational TSRs, the flow over the blade is more stable. Increased induction levels, accompanied with stronger velocity gradients, appear in the rotor plane. The velocity gradients are expected to influence the turbulent mixing of the wake into the outer flow, and vice versa. Furthermore, the helical structure of the near wake with tip and root vortices is affected. The operational TSR has a strong impact on the geometry of the near-wake flow field, and off-design TSRs stretch or compress the pitch of the helical wake structures. A denser helical structure at higher TSRs will affect the wake development with increased turbulence generation and increased mixing.

The DTU 10 MW rotor is aerodynamically suitable for the operation in the TSR range of approximately 5 to 10 to manipulate the wake. The operation at TSRs below and above the design TSR of 8 will result in a power production loss for the turbine. However, the modified, faster-recovering wake shall enable an increased power production for a downwind turbine. The goal is to optimize the net energy production of multiple waked turbines by balancing the power losses of the undisturbed turbine with the gains from the reduced wake losses incurred by a downwind turbine. The impact of the TSR on rotor aerodynamics and wake development is further investigated using LES and discussed in the following sections.

5 Single-turbine wake assessment

In the first stage of the LES, a TSR variation is carried out with a single DTU 10 MW turbine. A range between TSR 5 and 12 is covered. The simulated wind is uniform and non-turbulent with speed of 8 ms^{-1}. Although real turbines are subject to turbulent, sheared winds, in this study we simplify the problem to more clearly observe wake details that would otherwise be obscured in the background turbulence. It should be noted that it is established practice in aerodynamics to apply non-turbulent wind as a boundary condition in first investigations. In future studies, turbulent conditions will be studied.

The computational domain, with dimensions given in Table 2, is created by first constructing a uniform Cartesian mesh with hexahedral cells. We then add four successive refinement nests within the base mesh by selecting a region and cutting cells in half in each direction to double the resolution for each refinement nest. The grid resolution in the near-rotor vicinity has a grid resolution of 1 m in each direction. The resultant grid contains 21.2 million cells and is shown in Figure 3.

Table 2: Grid for single-turbine simulations

	x (m)	y (m)	z (m)
Minimum	-512	-640	-640
Maximum	2048	640	640

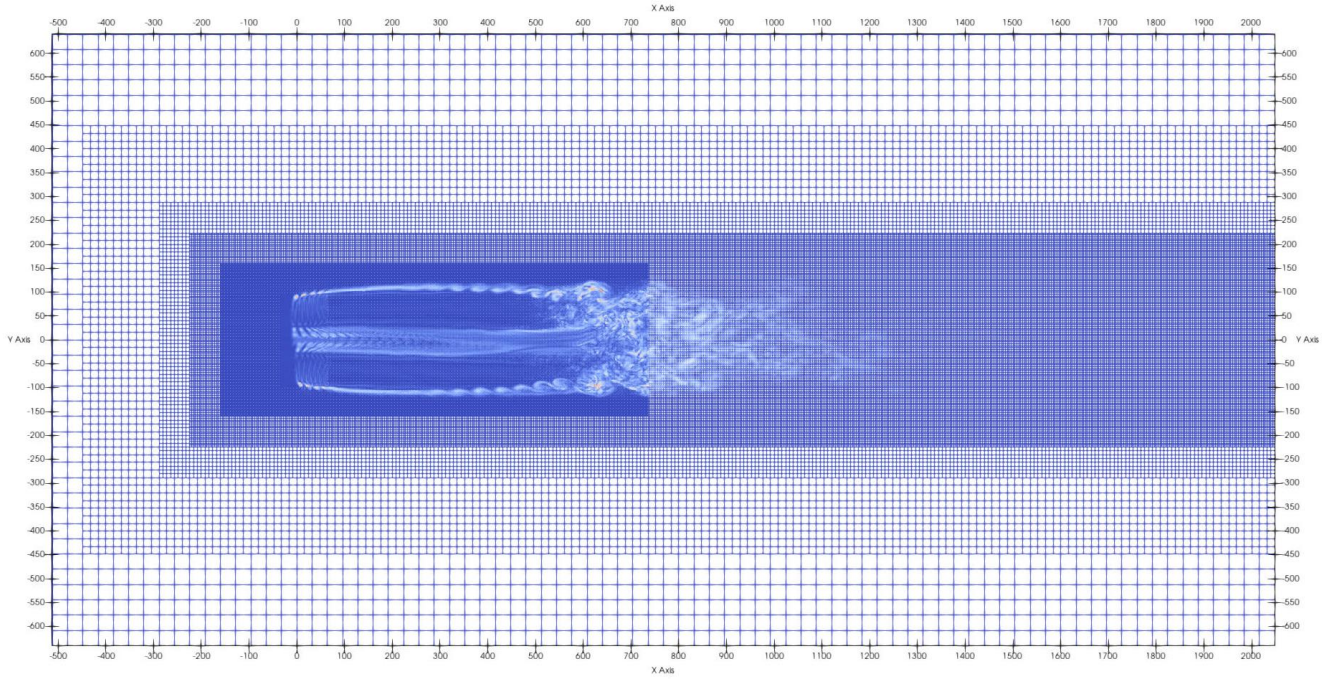

Figure 3: A horizontal cut through the mesh, showing the base mesh of 32 m resolution and the five nested refinement regions.

Postprocessing relies on the extraction of flow field data in horizontal and vertical slices as well as the extraction of time series data at many points in the wake. We extracted instantaneous and mean values of pressure, velocity, vorticity, and Q-criterion (the second invariant of the velocity gradient tensor). Given that the simulations are coupled with the OpenFAST tool, the full set of aeroelastic data is further available for all simulations.

The following data are used for the analysis:

- Turbine power production data
- Contours of wake velocity and vorticity in a horizontal cut plane through the computational domain
- Local horizontal wake velocity distributions
- Wake turbulence data

The variation of the TSR affects the power production of the turbine and the velocity distribution in the wake, as shown in Figure 4. The simulation data demonstrate that downwind wake velocities depend on the TSR.

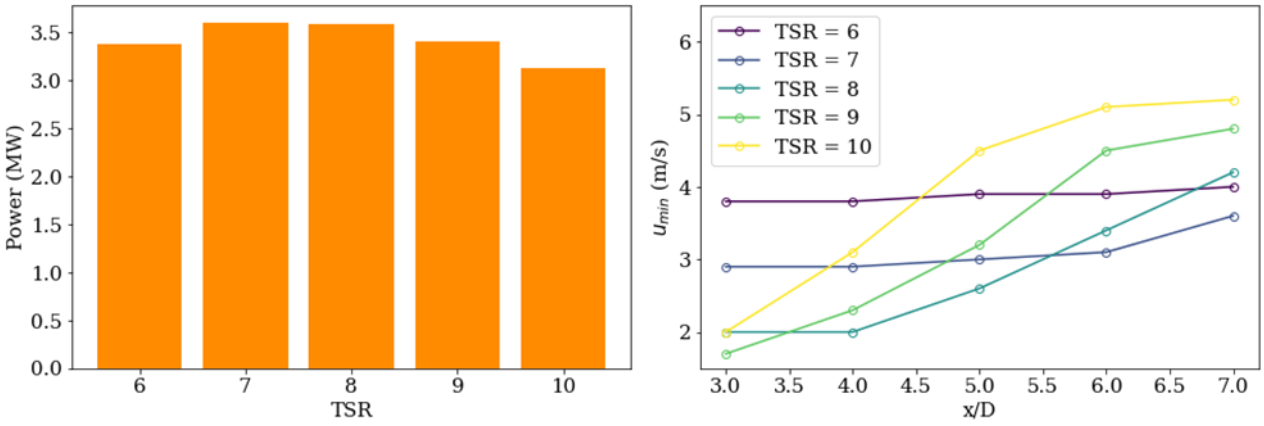

Figure 4: Predicted single-turbine power production (left) and wake velocity development (right) as a function of TSR from OpenFAST-coupled LES.

The DTU 10 MW turbine is designed to operate at a TSR of 7.5. For the operational range from TSR = 5 to TSR = 12 the resultant wakes are shown in Figure 5 and Figure 6.

The figures show contours of instantaneous velocity and vorticity magnitude in a horizontal plane cutting through the rotor hub. The low-TSR operation at a TSR of 6 results in decreased energy production, and therefore a less intense wake deficit, as shown in Figure 5. The low-induction operation creates comparatively high wake velocities, but the power production of the turbine is not favorable. The wake at a TSR of 6 is weak and stable and contains a low amount of turbulence, which can be quantitatively visualized by vorticity magnitude in Figure 6. With increasing TSR, the power production, wake deficit, and wake turbulence increase, as shown in Figure 5 and Figure 6.

The turbine is most efficient in the TSR range from 7 to 8. With highest efficiency, the wake deficit is substantial. Qualitatively, the magnitude of turbulent fluctuations appears higher compared to the low-TSR wake. An important effect of the increased wake turbulence is enhanced wake mixing and recovery.

In the TSR range from 9 to 10, power production starts to decrease slightly. The wake structure shows a strong turbulence development. The strong turbulence appears to provide the mixing to re-energize the wake within a short downstream distance, followed by dissipation of the turbulence.

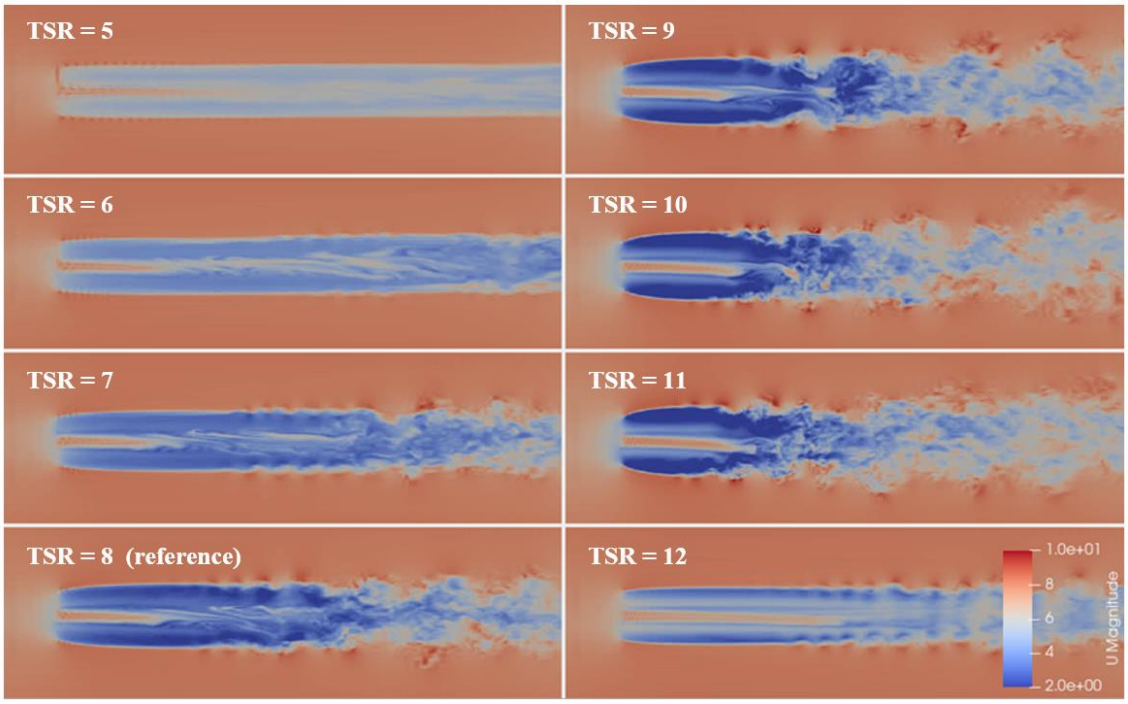

255 **Figure 5: Velocity distributions for the DTU 10 MW turbine operating at TSRs ranging from 5 (top left) to 12 (bottom right).**

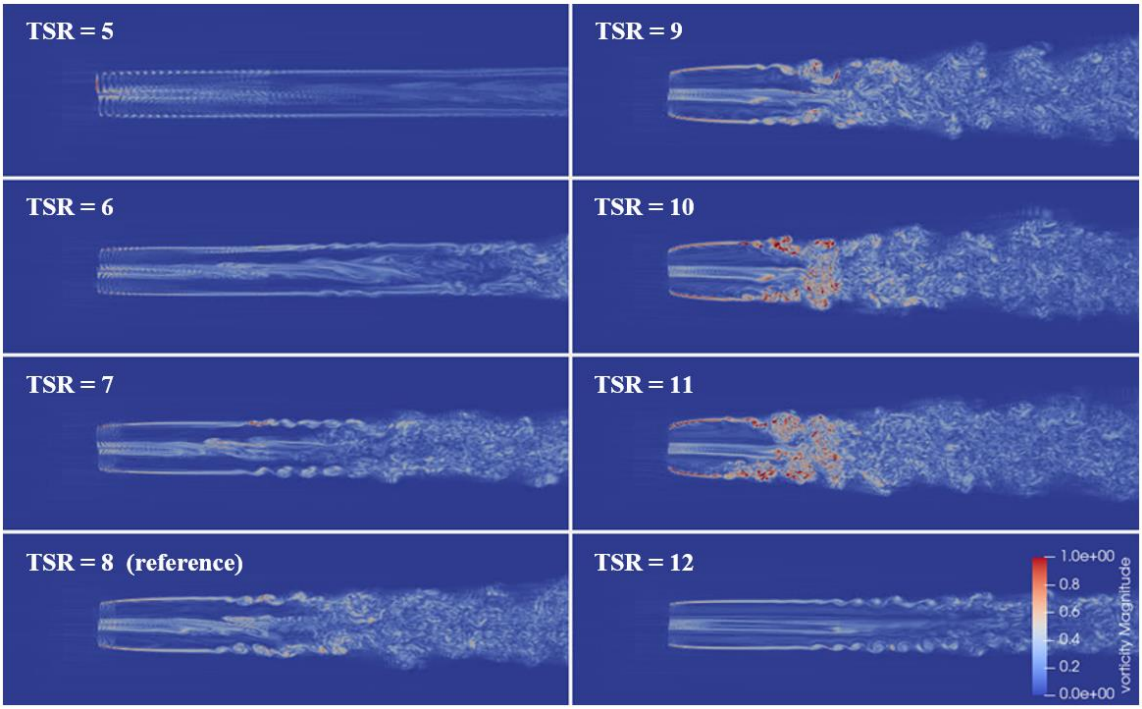

Figure 6: Vorticity distributions for the DTU 10 MW turbine operating at TSRs ranging from 5 (top left) to 12 (bottom right).

Turbulence development is vital for the wake recovery and our examination of turbulence to this point has been qualitative through examination of the instantaneous velocity field. Therefore, quantitative turbulence data are extracted and analyzed. The velocity vector components for 10 downwind points at x = 1 rotor diameter (D) to 10 D, y = 0.67 R (where R is the the rotor radius), and z = 0 in the wake are used to estimate local turbulent kinetic energy (TKE). The radial coordinate is at two-thirds the rotor radius. Data from t = 400 s to 600 s are used and statistical properties are estimated. TKE is a good indicator of mixing effects, and it is defined as half the sum of the variances σ^2 (square of standard deviations σ) of the fluctuating velocity components:

$$TKE = \frac{1}{2}(\sigma_u^2 + \sigma_v^2 + \sigma_w^2)$$

The derived TKE data are given in Figure 7. Variation of the TSR clearly influences the TKE development. The operation of the rotor at low TSRs generates low levels of TKE where values start to increase far downstream from 8 D to 10 D.

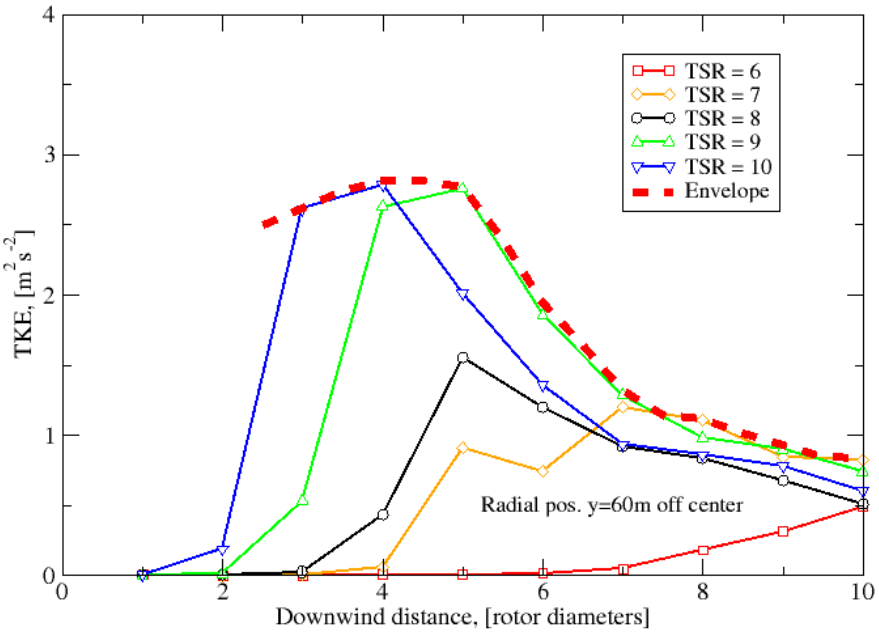

Figure 7: TKE downwind development for the range of TSRs from 6 to 10, at 2/3R in y-direction.

Increasing the TSR establishes a region with stronger turbulence in the wake. As TSR is increased, the position of peak TKE moves closer to the rotor. As for TKE strength and location, the existence of an envelope is likely. It can initially be taken from the TKE slopes and the locations of TKE maxima. Such an envelope, describing a possible operation range for TSR modifications and their impact on TKE magnitude and location, is shown in Figure 7.

For the investigated range of TSRs, it can be stated that high-TSR operation increases turbulence generation. The turbulent mixing effects have a positive influence on wake recovery, and hence increase the velocity that would be experienced by downstream turbines. This is evaluated further, and results for downwind wake velocities are given.

5.1 Wake velocity development as a function of the TSR

In Figure 8, wake velocity profiles at 2 D, 4 D, 6 D, 8 D, and 10 D downstream of the turbine are given for TSRs from 6 to 11. The results show that the turbine operation at different TSRs triggers different wake development patterns.

The operation of the turbine at a lower-than-rated TSR generates a moderate but very stable downwind velocity distribution. For very low TSRs, the wake is narrow and has low turbulence, and mixing effects are largely absent. Here, the wake recovery is slow, velocity minima stay at approximately 5 ms^{-1} up to 10 D downwind. The wake development is accompanied by the rotor producing 30% less power than ideal, as shown in Table 5.

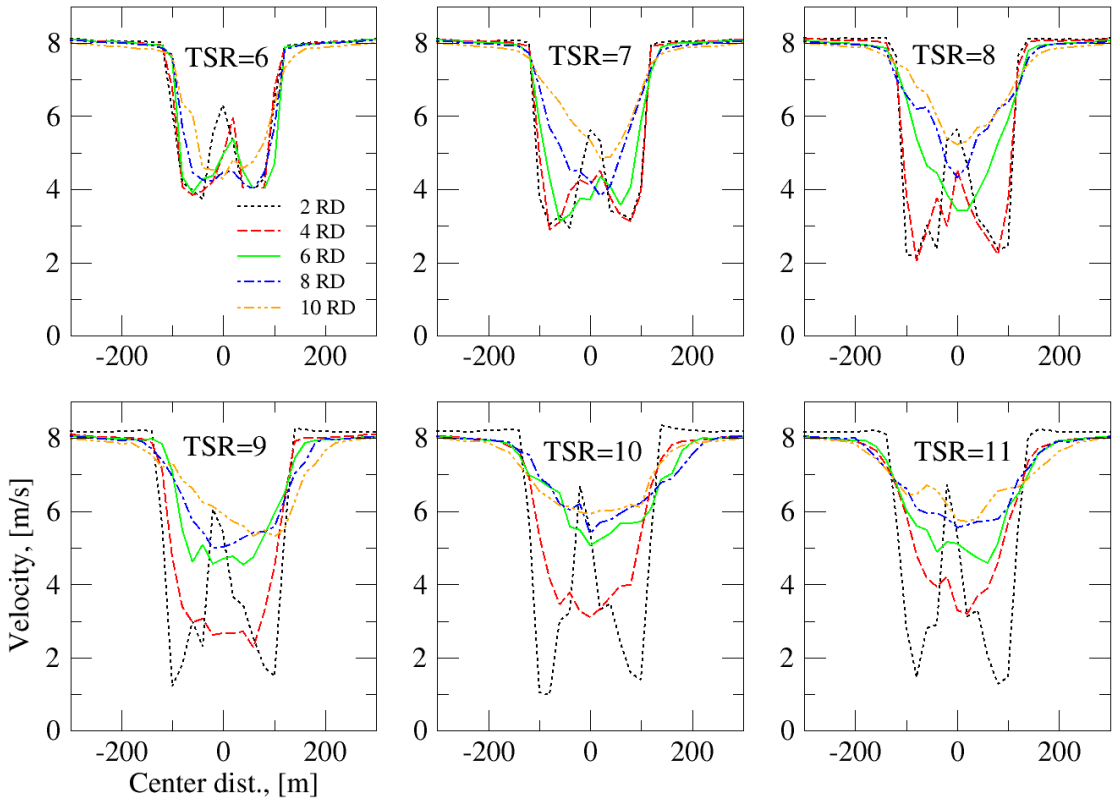

Figure 8: Mean velocity profiles along a horizontal, spanwise line at hub height as a function of increasing downwind distance for different TSRs.

The operation at (or near) the design point at a TSR of 8 results in a strong wake deficit, even in the near wake and up to 6 D downstream. This is the typical wake recovery seen with turbines operated as designed. Velocity minima in the center of the wake increase from 2.3 ms^{-1} in the near wake to 5.5 ms^{-1} at approximately 10 D downstream. The turbine is at its maximum efficiency in the TSR range from 7 to 8, and strong wake effects are present.

High-TSR operation establishes a different wake development with more turbulence and mixing effects closer to the rotor. The velocity variation from the near wake to the far wake is large. If the turbine is operated at a TSR of 9 to 11, velocities in the near-wake center are less than 2 ms^{-1}, and large velocity gradients appear. These gradients enhance turbulence development and mixing effects with the freestream flow. At medium distances from 6 D to 10 D, the wake recovers faster compared to lower-TSR operation, with wake centerline velocities between 5 and 6 ms^{-1}. The better wake recovery compared to the operation at the design point TSR causes a slight decrease in power performance. For example, the turbine efficiency is reduced by 5.6% for the operation at a TSR of 9.

The simulations reveal that velocity profiles in the wake can be controlled by a variation of the TSR. Low TSRs create moderate and very stable wakes, whereas high TSRs establish a much more dynamic wake development with enhanced wake recovery. These results support the goal of balancing power losses of the first turbine due to off-design operation with increased power production of downwind turbines through altered wake behavior.

5.2 Local wake control with the TSR

The simulation results presented in Figure 9 show the impact of the TSR on the mean wake for the downwind position at x = 6 D, a spacing on the low end of typical within a wind farm. The local mean velocity profile shows large wake velocity variations as a function of the operational TSR of the turbine. The comparison of the local profiles allows a first, qualitative identification of favorable TSRs to establish high wake flow recovery.

The operation at a TSR of 6 leads to unfavorable results for this position; wake velocity minima are in the range of 3.2 ms^{-1}. That is the lowest estimated velocity here. Increasing to a TSR of 7 results in a slightly better velocity recovery; here, minima around 3.9 ms^{-1} appear. For operation with TSR of both 6 and 7, the wake shape has a velocity peak in the center. Standard operation is at TSR of 8 (black), where the wake has a Gaussian-like shape; the velocity minimum is at 3.4 ms^{-1}. All operation for TSR > 8 increases wake recovery. TSRs of 9, 10, and 11 show significantly increased velocity recovery. For TSRs of 9, 10, and 11, the velocity minima are 4.5 ms^{-1}, 5.2 ms^{-1} ms^{-1}, and 4.3 ms^{-1}, respectively.

For the downwind distance of 6 D, the best wake flow development is observed for a TSR of 10. The velocity recovers faster than for all other TSRs. For a TSR of 10, the power production is 3199 kW. The operation at a TSR of 9 gives the second-best recovery and a power production of 3400 kW. For a two-turbine array with a turbine distance of 6 D, the operational TSR range from 9 to 10 seems beneficial to increase wake recovery and optimizes the power production of the waked turbine. This conclusion, though, is based on wake flow data from a single turbine. For a detailed assessment, we simulate a second turbine in the respective wake position, as discussed in Section 6.

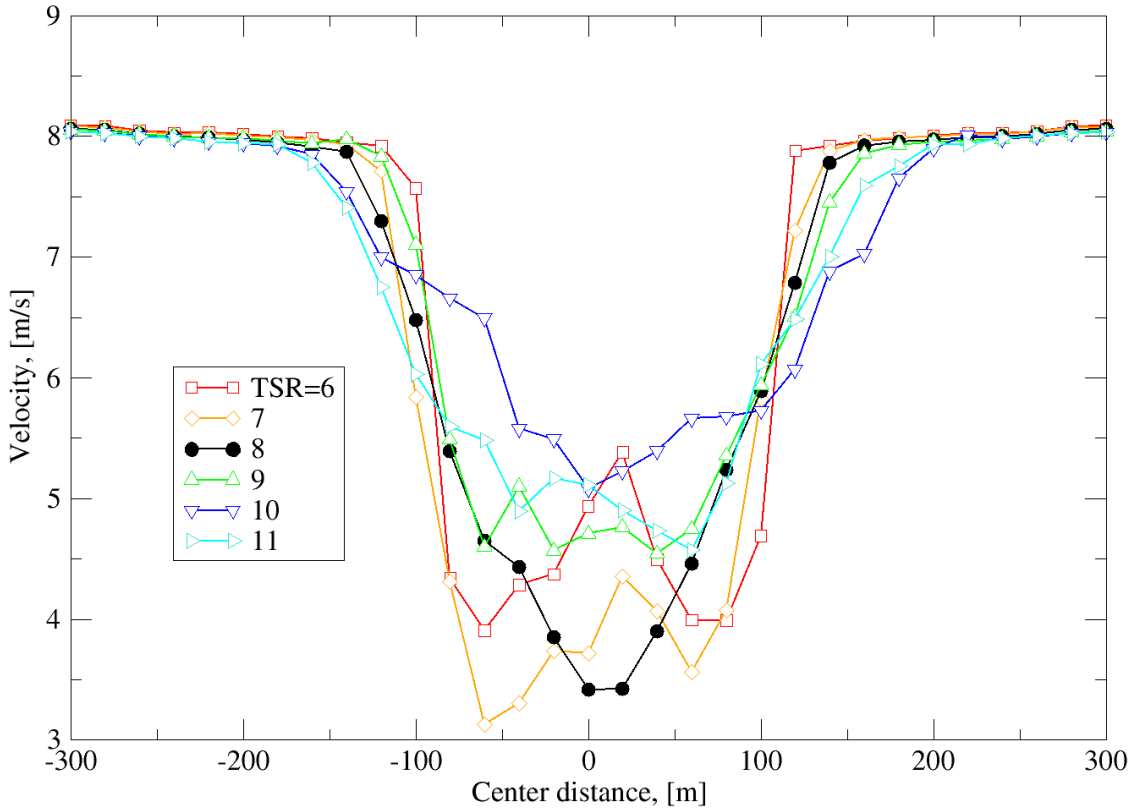

335 **Figure 9: Mean velocity profiles along a horizontal, spanwise line at hub height at x = 1070 m (6 D) downstream as a function of TSR.**

5.3 Turbulence development

A main feature of a wake is the turbulence development. Wake turbulence data from the simulation of the DTU 10 MW turbine
340 at TSRs 6, 8, and 10 are analysed. Velocity time histories are extracted at 6D downstream and 2/3R radially outward from the rotor center. The data at 2/3 of the rotor radius are regarded as representative for the aerodynamics with impact on power production and loads.

In Figure 10, the development of the resulting flow vectors (from x, y, z components) are given in the left diagram. The spectra of the time history of the velocity vectors are derived from 300 s to 600 s data and are shown in the diagram on the right. The operation at a TSR of 6 results in a wake development with low velocity and very little turbulence at 6D. The spectral content for a TSR of 6 is mainly located between 0.1 Hz and 0.2 Hz. The less turbulent wake is not optimal to establish turbulent mixing but might reduce turbulence-induced loads for a second turbine in the wake.

At TSRs of 8 and 10, a full developed turbulent wake with higher wind speeds and turbulence is established. A better wake velocity recovery for the operation at a TSR of 10 is visible. Spectral data show a slightly different behavior for a TSR of 8 and a TSR of 10. For the lower TSR of 8, energy in the spectrum around 0.1–0.2 Hz increases slightly compared to that of the operation at TSR of 10. The turbulence intensity at a TSR of 10 is somewhat reduced, as summarized in Table 3. It seems that the turbulence intensity is dominated by the frequency range from 0.01 Hz to 0.3 Hz. The results indicate an interesting potential of high-TSR operation of upstream turbines to create both a turbine power production increase and a load reduction for downwind turbines.

Table 3: Turbulence data at x = 6D, y = 2/3R.

	TSR = 6	**TSR = 8**	**TSR = 10**
Average velocity, [ms^{-1}]	4.53	5.55	6.45
Std. dev. Velocity, [ms^{-1}]	0.17	0.93	0.97
Turbulence intensity, [-]	3.7%	16.7%	15%

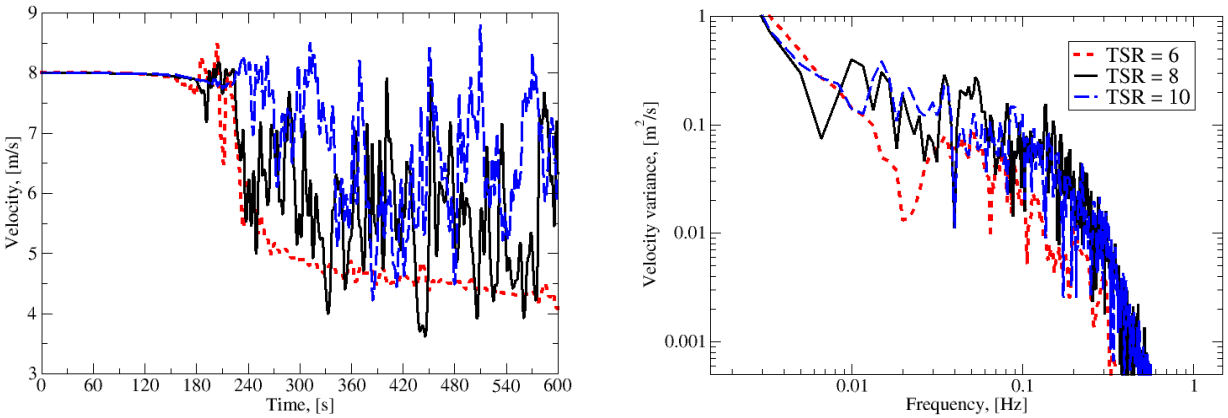

Figure 10: Velocity time history (left) and velocity spectra (right). Spectral distributions are estimated from time window of 300 to 600 s.

6 Wake simulations for two turbines

Given that the objective of TSR control of wakes is to improve performance of a set of wind turbines in which the wind direction causes waking, we present a detailed assessment of the impact of TSR variation on the wake development and the combined power production based on LES with a two-turbine-array, again using the DTU 10 MW turbine modelled in OpenFAST.

The two turbines in the array have different tasks: the first turbine shall modify its wake through a TSR variation. The second turbine in the wake shall produce a maximum amount of energy. Only the TSR of the first turbine is varied. The operational speed of the second, downwind turbine in the wake is set to the design TSR of 8, where its performance is optimal. This ensures a clear identification of the impact of the operational TSR of the first turbine on the power production of the second turbine. Sets of TSR variations from 5 to 11 for the first turbine are simulated with a turbine spacing of 6 D.

LES allows for the detailed estimation of the impact of TSR on the power production of the upstream turbine and on the wake development and resulting power production of the downstream turbine. The target is to optimize the combined energy production of the two turbines as a function of the TSR of the first turbine. TSRs for maximum power production are identified for the investigated 6D spacing.

6.1 Simulations

The computational domain was slightly enlarged in width and height and considerably lengthened in the flow direction compared to the single-turbine simulations. The dimensions of the computational domain are given in Table 4. The hexahedral grid is refined 5 times, with a minimum cell size of 1 m in the turbine/wake-local area. The grid contains 42.3 million cells. The first turbine is positioned at x = 0; the second turbine is located at 1070 m (6 D downstream). For turbulence modelling, the Smagorinsky LES model is applied (Smagorinsky, 1963). A simulation time step size of 0.01 s is set such that the Courant–Friederichs–Lewy number is less than 1. The spatial and temporal resolution in the simulation is regarded as sufficiently high, because more than 80% of the turbulent energy in the wake is captured, and typical flow features like tip and root vortices are resolved.

Table 4: Grid dimensions for two-turbine simulations

	x (m)	**y (m)**	**z (m)**
Minimum	-512	-992	-992
Maximum	4608	992	992

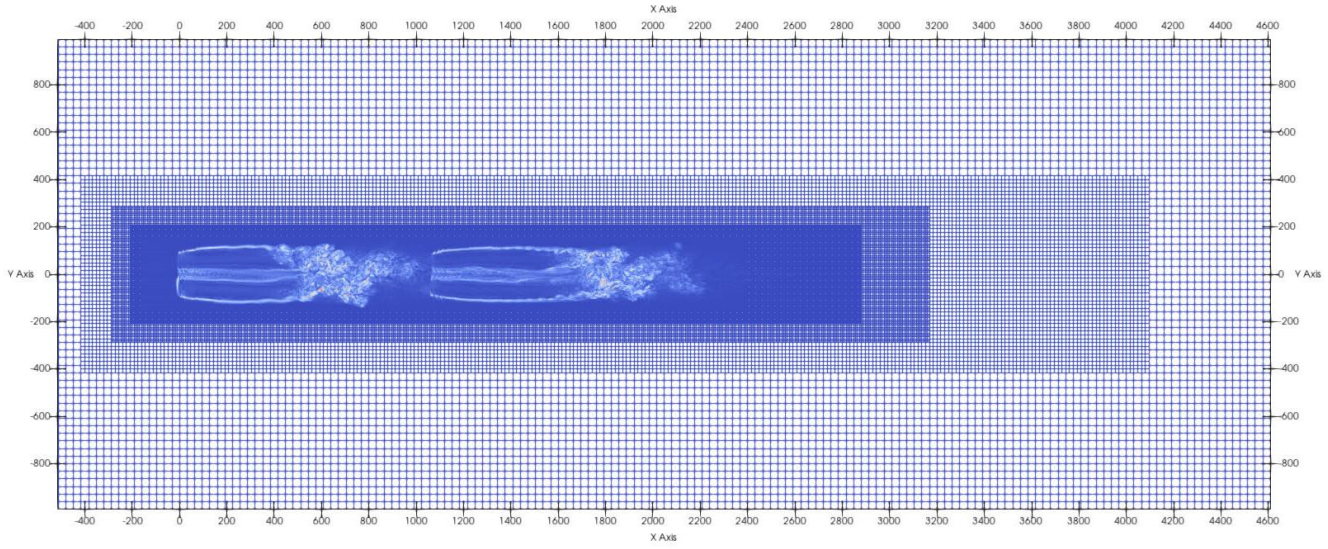

Figure 11: Grid for two-turbine simulations with turbine positions. Turbine 1 is at origin, Turbine 2 is located 6 D downstream (1070 m).

6.2 Simulation results for a two-turbine array

The simulations were carried out with two-turbine arrays with inter-turbine distances of 6 D. For each array, a TSR variation from 5 to 11 was carried out for the first turbine, and the second turbine in the wake was always operated at a TSR of 8. Due to the non-linear behavior of rotor aerodynamics, some deviations were observed. When we intended to simulate a TSR of 5, an actual TSR of 4.6 was realized, and intended runs with TSR of 11 resulted in a realized TSR of 10.3. For both very low and very high TSRs, the rotor torque generation changes because large angle of attack changes appear. These, in addition to the effect of the rotational speed, generate a power/rpm curve which deviates from the simple implemented generator model. Typical results from the simulations from the array with 6 D (1070 m) turbine distance are given in Figure 12 and Figure 13. The figures show instantaneous velocity and vorticity distributions in horizontal planes at hub height at t = 600 s.

6.2.1 Low-TSR operation

The top diagram in Figure 12 shows the flow development for a low TSR of 4.6 for the first turbine. The low-TSR operation extracts less energy from the wind compared to the operation at the design TSR in the range from 7 to 8. The power production of the first turbine is 3.17 MW. The wake behind this turbine exhibits low turbulence development. Turbine 2 has a power production of 1.67 MW. The near wake of Turbine 2 shows a very strong velocity reduction and a strong vorticity development in the outer radial regions of the rotor. The wake development for Turbine 1 operation at a TSR of 6 is similar to the TSR of

4.6 case. The inner part of the first wake shows some turbulent structures, but no strong mixing effects take place. The power production of the first and second turbines are 3.37 MW and 0.64 MW, respectively. Turbine 2 creates a strong wake where additional downstream meandering appears.

415

6.2.2 Standard TSR operation

The two diagrams in the middle of Figure 12 and Figure 13 show the wake development for standard operation. The first turbine operates here at TSRs of 7 or 8. For a TSR of 7, the wake of the first turbine (operating at a power of 3.6 MW) is not yet fully turbulent when it reaches the second turbine. This might be a reason for the massive power production drop of Turbine 2. The first turbine extracts a maximum of energy from the flow, but the wake lacks turbulent mixing and is only partly re-energized. The power production for Turbine 2 is only 0.454 MW. For a TSR of 8, the flow develops in a similar fashion. Power production for the first and second turbines is 3.58 MW and 0.633 MW, respectively. The slight increase in the power production of Turbine 2 compared to the TSR of 7 result seems to be related to increased turbulent mixing, as turbulent patterns appear earlier. In general, wake effects are substantial for TSRs 7 and 8, with the second turbine's power production reduced to 12.5 % and 17.7 %, respectively.

420

425

6.2.3 High-TSR operation

The operation at TSRs beyond the design TSR of 8 is investigated. We simulate a range of TSRs of 9, 10, and 11, and results are shown in the lower diagrams of Figure 12 and Figure 13. The velocity and vorticity distributions show a clear trend: The development of more and more turbulent flow structures in the wake of the first turbine is related to the increasing TSR. High TSRs establish more turbulence and an increased mixing with the outer flow. The power production of the first turbine decreases for higher TSRs. But the power production of the second turbine increases significantly. If the first turbine is operated at a TSR of 9, its power production is 3.4 MW (a reduction of 200 kW relative to the reference simulation). The second turbine produces 1.36 MW (an increase of 727 kW relative to the reference simulation). Detailed results for resulting power productions are given in Figure 14 and Table 5 (both for 6 D distance).

430

435

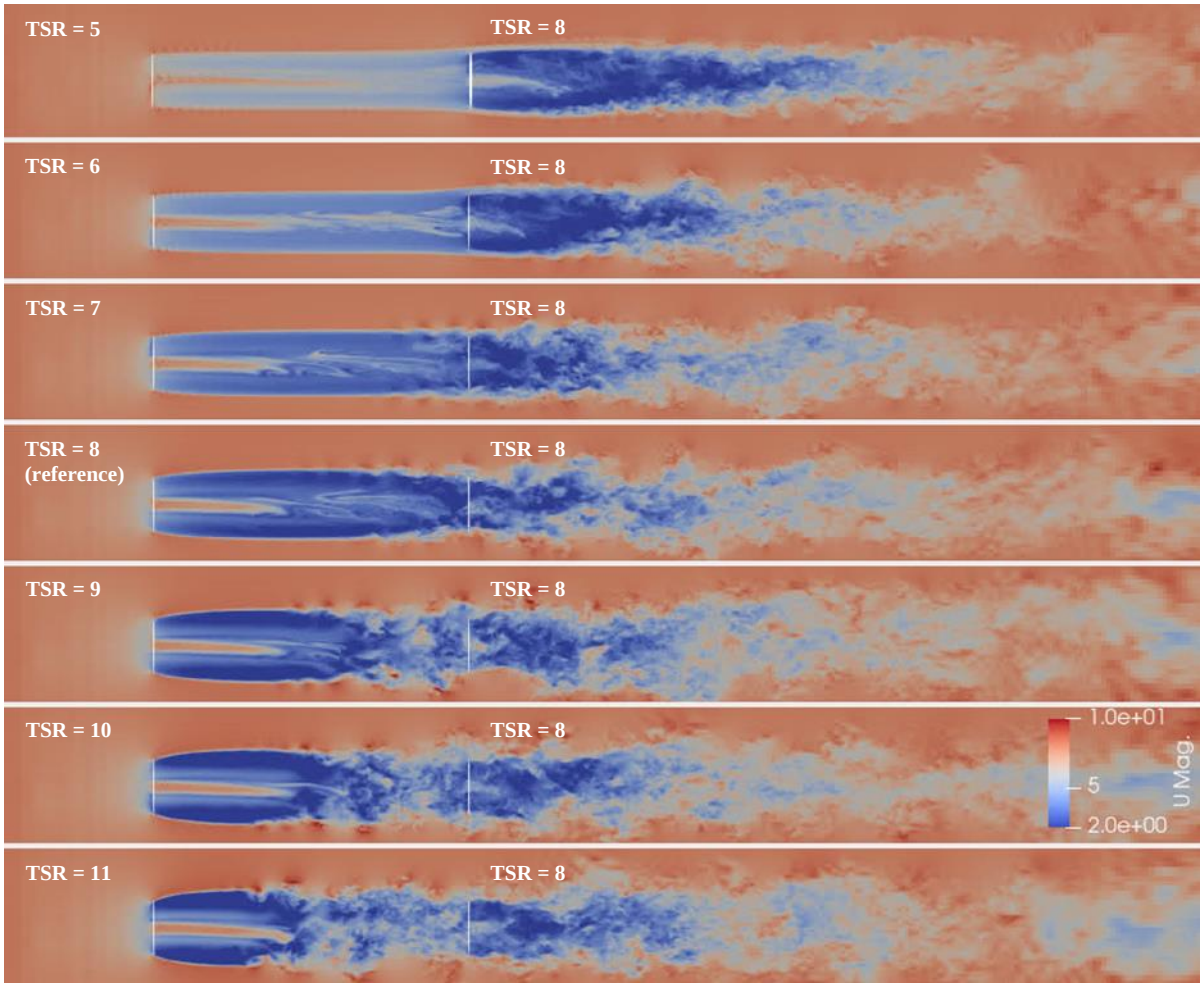

Figure 12: Velocity distributions for two turbines. The first turbine is operated at TSRs from 5 (top) to 11 (bottom), and the second turbine is operated at a TSR of 8. Turbine distance is 6 D.

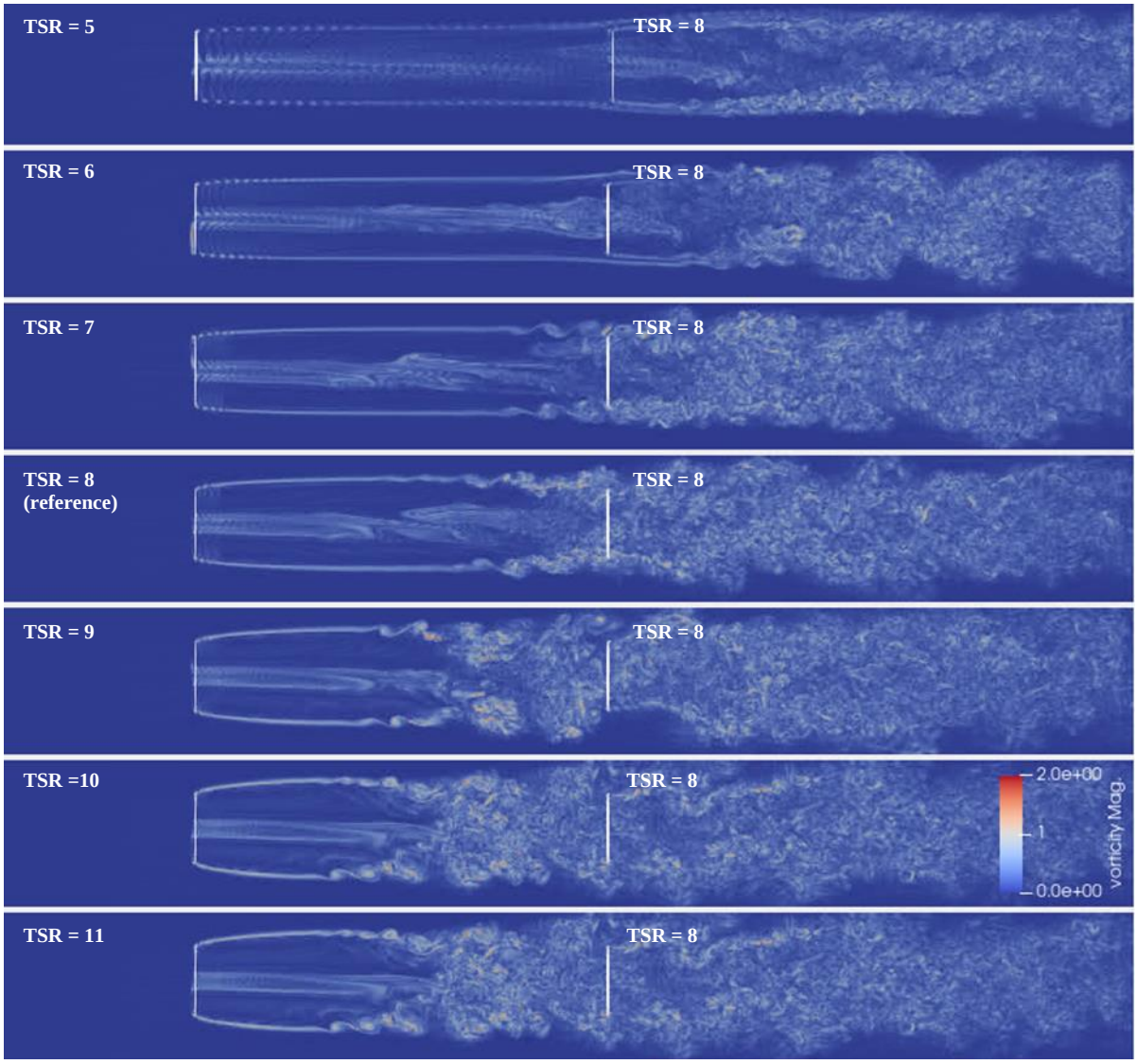

Figure 13: Vorticity distributions for two turbines. The first turbine is operated at TSRs from 5 (top) to 11 (bottom), and the second turbine is operated at a TSR of 8. Turbine distance is 6 D.

445

For the array with 6 D (1070 m) turbine distance, the resulting power production as a function of TSR is given in Figure 14 for both turbines, which shows the development over the simulation time. In the simulations, turbine operation is started with a fixed rpm in an even wind field of 8 ms^{-1} in the whole computational domain. The wake flow fields are established in the first 100 s of the simulation and start to arrive 6 D downstream at the downwind turbines after 150 s. A stationary wake flow
450 pattern is established after approximately 360 s. The power production for all upwind turbines is smooth due to the incoming deterministic wind at 8 ms^{-1}.

The power production of the downwind turbines shows different behavior: If the first turbine is operated at a TSR of 4.6, the second turbine has smooth power production due to the wake with very low turbulence. The low efficiency of Turbine 1 operating at a TSR of 4.6 leaves a lot of energy in the wake, so the power production of Turbine 2 is high. The power production for TSRs in the range from 6 to 8 is high for the first turbine and dramatically lower for the turbine in the wake. The production here shows little variation in general. For higher TSRs of 9 and 10, power production of the first turbine is reduced, but the power production of the waked turbines compensates the loss, and an overall production increase is realized. The increased power production of the waked turbines shows some low-frequency dynamics. Averaged power production data for all configurations are given in Table 5.

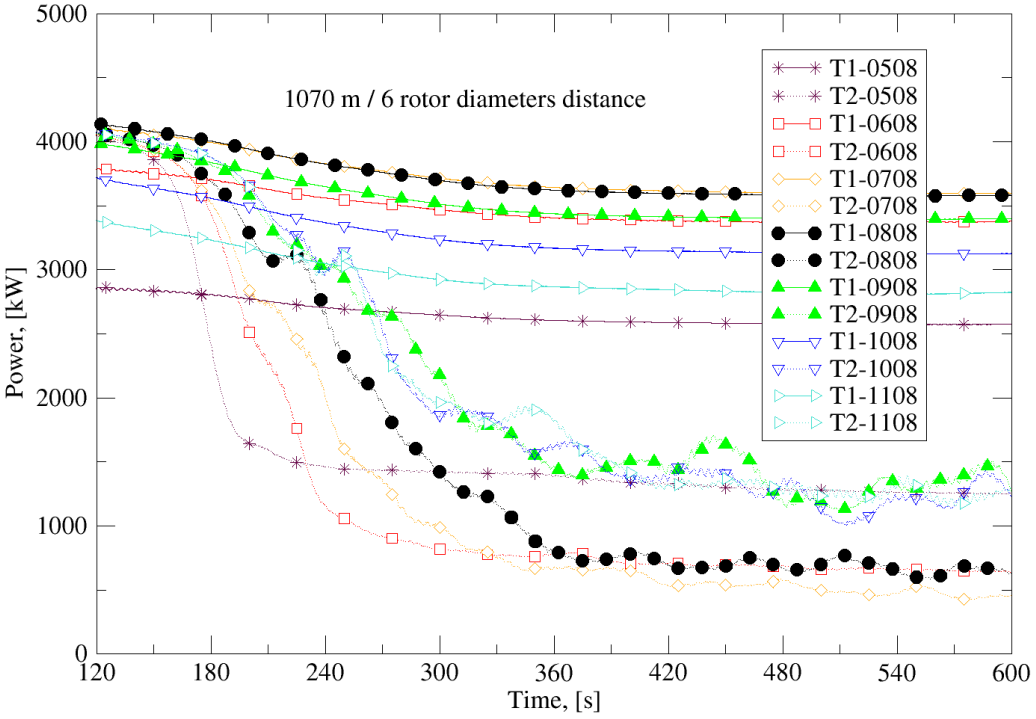

Figure 14: Time history of power generation for two-turbine arrays spaced 6 D apart. The term T1-0508 is Turbine 1 power from the simulation with Turbine 1 at a TSR of 5 and Turbine 2 at a TSR of 8.

Table 5: Power productions for TSR variation for Turbine 1 and a constant TSR of 8 for Turbine 2 from LES. Turbine distance is 6 D.

TSR Turbine 1 [-]	Power Turbine 1 [kW]	TSR Turbine 2 [-]	Power Turbine 2 [kW]	Combined Power Production [kW]
5 (4.6)	2573.9	8	1245.3	3819.2
6	3378.6	8	642.9	4019.7
7	3598.8	8	454.1	4052.9
8	3581.9	8	633.2	4215.1
9	**3399.3**	**8**	**1363.7**	**4763.0**
10 (9.7)	3126.0	8	1266.9	4382.9
11 (10.3)	2823.2	8	1230.4	4053.6

The parameter studies identified alternative TSRs for the first turbine which increased the combined power production for the two turbines (see Figure 14 and Table 5).

To increase the production of the array, the spacing between the turbines is key for the choice of the TSR:

- For short spacings up to 4 D, the first turbine might be operated at a low TSR < 7.
- For larger spacings greater than 4 to 5 D, a higher TSR > 8 for the first turbine is beneficial.
- For very large inter-turbine spacings, the wake might not be controlled; in this case, both turbines should be operated at design TSR for maximum power production.

In Figure 15, the power production for a two-turbine array with an inter-turbine distance of 6 D is shown. The TSR of the first turbine is varied from a TSR of 4.6 to 10.3. The power production of the two turbines can be balanced and optimized by the TSR. For this short distance, a TSR of 9 gives an overall production increase.

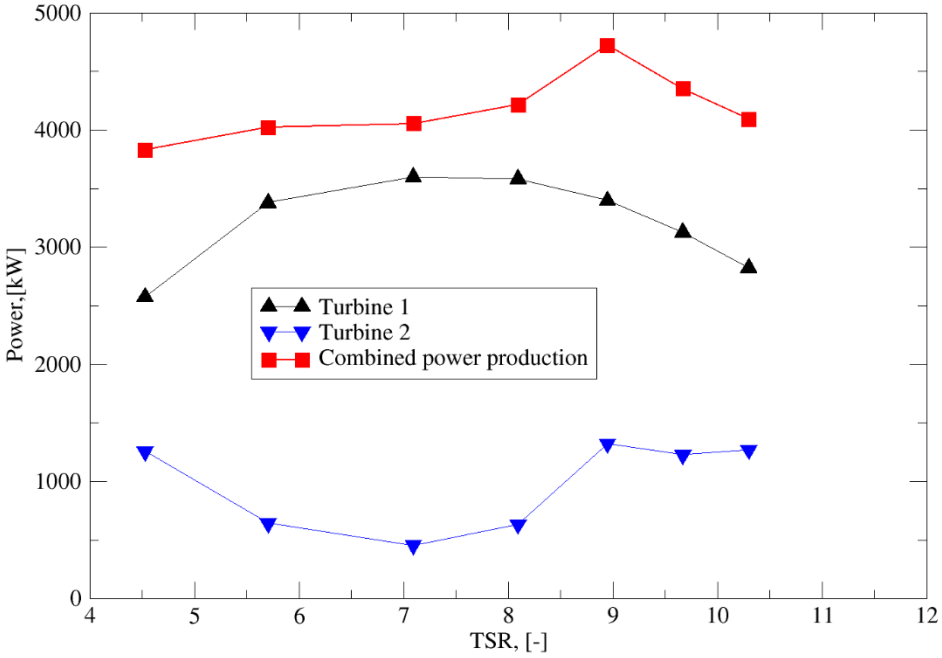

485 **Figure 15: Individual and combined turbine power production as function of TSR for turbine distance of 6 D (1070 m).**

The simulations highlight the potential benefits of flow control through a TSR adaptation. The incoming wake for a downwind turbine is a function of the distance to the upwind turbine and the operational TSR of the upwind turbine. The tuning of the operational TSR of the first turbine allows the optimization of the power production for the investigated two-turbine array.
490 The method is applicable to larger arrays of turbine – but the optimization process is different, in that the operational TSR of several turbines must be tuned.

7 Conclusion

The application of wake flow control measures can reduce wake losses in offshore wind farms. A comparative numerical analysis for wake control through of the adaptation of the operational TSR of wind turbines was carried out.
495

The flow through an offshore wind farm is complex because it is a mixture of aerodynamic and meteorological flow phenomena. Turbulence simulation is especially challenging, requiring high spatial and temporal resolution in a large

computational domain. We applied large-eddy simulation and turbine aeroelastic simulation to typical wind turbine wake scenarios.

First, TSR parameter studies with a single turbine were conducted. A large computational domain with the dimensions of 2.560 x 1.28 x 1.28 km containing 21 million grid cells with five grid refinements was used. A non-turbulent, non-sheared wind of 8 ms^{-1} was used as the inflow boundary condition. The DTU 10 MW reference turbine was utilized.

We conducted simulations in a range of distances, and the most relevant results were for a distance of 6 D. Parameter studies covered operational TSRs from 5 to 11. The studies distinctly showed the impact on the wake development of a large turbine. The variation of the operational TSR affects the power generation of the turbine and its wake characteristics. The two features have to be balanced such that an increased operational TSR creates a slight power loss of upwind turbines but results in a better wake recovery to enhance the energy production of downwind turbines. It was found that the operation of the DTU 10 MW turbine in the TSR range from 9 to 11 resulted in a general wake velocity increase at downwind distances larger than 3 D. Centerline wake velocities grew from 2.6 ms^{-1} to 4.5 ms^{-1} for the increase in TSR from 8 to 10.

The physical process introduced by a TSR variation is the modification of the turbulent development in the wake. A higher TSR brings strong turbulence development closer to the rotor; therefore, turbulent mixing starts to re-energize the wake nearer the rotor than with lower TSRs. The operation at a TSR of 10 establishes strong maxima of the TKE at 3 D to 4 D behind the turbine, whereas the operation at the design TSR of 8 results in weaker TKE maxima at 5 D. The general turbulence development for high-TSR operation seems to be advantageous; strong turbulence near the rotor provides strong mixing and re-energizing of the flow. This turbulence breaks down and reaches low intensity at distances of 7 D to 8 D.

In the second part of the investigation, a two-turbine array was investigated. Again, the DTU 10 MW turbine was used.
The larger computational domain had the dimensions 5.12 x 1.984 x 1.984 km and contained 42.3 million cells. The grid was refined 5 times. The first rotor was located in the center, the second rotor was positioned 1070m downstream.

A TSR parameter study was carried out. The TSR of the first turbine was varied in the range from 5 to 11. The second turbine in the wake was always operated at the design TSR of 8. This resulted in a distinct identification of the TSR impact on wake characteristics. The two-turbine simulations confirmed the results from the single-turbine simulations: the wake can be controlled by the operational TSR and wake recovery can be increased. With a second turbine operating in the wake, quantitative data regarding the power production were assessed.

The high-TSR operation of the first turbine at a TSR of 9 and standard operation of the second turbine at a TSR of 8 results in a combined power production of 4763 kW relative to the reference production of 4215 kW when operating both turbines at a

TSR of 8. The high-TSR operation increases the combined power production by 548 kW, or 13 %. In other words, at standard operation with a TSR of 8 for both turbines, the power production of the downwind waked turbine is 633 kW. If Turbine 1 is operated at a higher TSR of 9, the power production of the downwind turbine increases to 1364 kW, which is an increase of 115 %. The large power production gain for the downwind turbine is larger than the slight losses from high-TSR operation of the first turbine.

It is concluded that a tuning of the operational TSR of a turbine can be used to mitigate wake effects on downwind turbines. Through high-TSR operation of a turbine, the wake turbulence development can be used to enhance turbulent mixing and to re-energize the wake flow. Power production for downwind turbines can be increased substantially. The overall energy production of the investigated array with two 10 MW turbines is increased by 13% through a slightly higher-TSR operation of the upwind turbine.

Future work will focus on the application of the technique in realistic turbulent atmospheric boundary flows of different atmospheric stability and on the assessment of wake control as a function of both blade pitch and TSR. Furthermore, large turbine arrays will need to be tested for TSR tuning to mitigate wake losses.

Contributions

AK, LM, MC and SS identified and developed the method to modify the wake through a TSR adaptation. AK was responsible for the setup and conduction of simulations, analysis and writing. LM contributed to the cluster installation, operation and further discussion and analysis of results. MC supervised the SOWFA setup and the fine-tuning of simulation settings for parameter studies; he was further in charge of the technical review. SS contributed to the turbine modelling, the OpenFast setup and the technical review.

Competing interests

The contact author has declared that there are no competing interests for the authors of this publication.

Acknowledgements

This work was authored in part by the National Renewable Energy Laboratory for the U.S. Department of Energy (DOE) under Contract No. DE-AC36-08GO28308. Support for the work was also provided by Equinor Energy AS under Agreement 4503414590-CRD-16-00624. The views expressed in the article do not necessarily represent the views of the DOE or the U.S. Government. The U.S. Government retains and the publisher, by accepting the article for publication, acknowledges that the U.S. Government retains a nonexclusive, paid-up, irrevocable, worldwide license to publish or reproduce the published form of this work, or allow others to do so, for U.S. Government purposes.

References|

Adaramola, M.S. and Krogstad, P.Å. (2011). Experimental investigation of wake effects on wind turbine performance. *Renewable Energy, 36, 2078-2086, doi:10.1016//j.renene.2011.01.024*.

Badger et al. (2025, 20 05). *https://globalwindatlas.info/en/*. Retrieved 01 20, 2025, from Global Wind Atlas: https://globalwindatlas.info/en/

Bak et al. (2012). Light Rotor: The 10-MW reference wind turbine. *Proceedings of EWEA 2012 - European Wind Energy Conference & Exhibition.* Copenhagen: EWEA.

Barthelmie et al. (2009). Modelling and measuring flow and wind turbine wakes in large wind farms offshore. *Wind Energ., 12: 431- 444. Special Issue: Offshore Wind, doi:10.1002/we.348*.

Boersma et al. (2017). A tutorial on control-oriented modeling and control of wind farms. *Proceedings of the 2017 IEEE American Control Conference (ACC)* (pp. 1-18, doi:10.23919/ACC.20177962923). Seattle, WA, USA: ACC.

Bossanyi, E. and Ruisi, R. (2021). Axial induction controller test at Sedini wind farm. *Wind Energ. Sci., 6, 389–408, doi: 10.5194/wes-6-389-2021*.

Churchfield, M. (2024, 10 14). *https://www.nrel.gov/wind/nwtc/sowfa.html*. Retrieved from https://www.nrel.gov: https://www.nrel.gov/wind/nwtc/sowfa.html

Fleming et al. (2022). Serial-Refine Method for Fast Wake-Steering Yaw Optimization. *J. Phys.: Conf. Ser. 2265 032109, doi:10.1088/1742-6596/2265/3/032109*.

Grötzbach, G. (1987). Direct numerical and large eddy simulation of turbulent channel flows. In N. Cheremisinoff, *Encyclopaedia of Fluid Mech., vol. 6* (pp. 1337-1391). Houston: Gulf Publication.

Houck, D. R. (2022). Review of wake management techniques. *Wind energy*, 195-220.

Jonkman, J. (2024, 10 14). *https://www.nrel.gov/wind/nwtc/openfast.html*. Retrieved from NREL web site: https://www.nrel.gov/wind/nwtc/openfast.html

Marten, D. (2024, 10 14). *https://qblade.org/*. Retrieved from Qblade web site: https://qblade.org/

Méchali et al. (2006). Wake effects at Horns Rev and their influence on Energy production. *Proceedings of 2006 European Wind Energy Conference and Exibition.* Athens: EWEA.

Moeng, C. H. (1984). A large-eddy simulation model for the study of planetary boundary layer turbulence. *J. Atmos. Sci. 29*, 2052-2062.

Munters, W. and Meyers, J. (2018). Dynamic strategies for yaw and induction control of wind farms based on large-eddy simulation andoptimization. *Energies, 11 (1), Article 177. doi:10.3390/en11010177*.

OpenCFD. (2025, 06 10). *www.openfoam.com*. Retrieved from OpenFOAM, the open source CFD toolbox: https://www.openfoam.com/

Porté-Agel, F. and Dillip, D. (2017). Wind Turbine Wake Mitigation through Blade Pitch Offset. *Energies 10. 757. doi: 10.3390/en10060757*.

Réthoré et al. (2011). *TOPFARM wind farm optimization tool.* Risø National Laboratory for Sustainable Energy, Technical University of Denmark, Denmark.

Rott et al. (2018). Robust active wake control in consideration of wind direction variability and uncertainty. *Wind Energy, 3, 869-882, doi:10.5194/wes-3-869-2018.*

Schumann, U. (1975). Subgrid scale model for finite difference simulations of turbulent flows in plane channels and annuli. *J. Comput. Phys., 18*, 376-404.

Sebastiani et al. (2021). Data analysis and simulation of the Lillgrund wind farm. *Wind Energy*, 24: 634-848.

Smagorinsky, J. (1963). General Circulation Experiments with the Primitive Equations. *Monthly Weather Review*, 99-164.

Thomsen, K. and Sørensen, P. (1999). Fatigue loads for wind turbines operating in wakes. *Journal of wind engineering and industrial aerodynamics*, 121-136.